OPTICAL AND ELECTRICAL PROPERTIES OF A-Si:H MULTILAYER SOLAR CELLS

A Thesis Submitted to the
School of Graduate Studies of
Addis Ababa University

In Partial Fulfilment of the Requirements
for the Degree of Master of Science
in Physics

ADDIS ABABA UNIVERSITY

BY
BELAYNEH MESFIN

JUNE 1998
ADDIS ABABA

Addis Ababa University

School of Graduate Studies

OPTICAL AND ELECTRICAL PROPERTIES OF A-Si:H MULTILAYER SOLAR CELLS

By

BELAYNEH MESFIN

Department of Physics

Faculty of Science

ADDIS ABABA UNIVERSITY

APPROVED BY THE EXAMINATION COMMITTEE:

Dr. Ulrich Stutenbaeumer
(University advisor)

Dr. Bantikassegn Workalemahu
(Examiner)

Dr. Araya Asfaw
(Examiner)

To

W/o Alganesh Agegnehu

and

Ato Nigatu Agegnehu

Acknowledgements

I would like to express my heart felt gratitude to my advisor Dr. Ulrich Stutenbaeumer for his consistent assistance, invaluable guidance and friendly encouragement without any reservation throughout my research work.

I am very grateful to the staff members of the Physics Department of the Addis Ababa University who in one way or another supported in facilitating my work. In particular, I would like to express my appreciation to Ato Amensisa Abdi who provide me with reading materials.

I am very grateful to my friends Alemna Jaleta and Solomon Beneberu for their consistent encouragement throughout my study program.

Last but not least, I would like to thank my sister Seblewongel Mesfin for making life easy during my study.

Contents

ABABA UNIVERSITY

List of tables

List of figures

Abstract

The transmittance spectra of a-Si:H pin solar cell samples having different i-layer thickness were measured with a Perkins Elmer Lambda 19 spectrometer. The spectra were simulated with the SCOUTFIT computer program by making use of the Forouhi and Bloomer dielectric function model to determine the values of the optical parameters (energy gap, refractive index and layer thickness) of the different layer systems (glass, TCO, p-, i- and n-layers) of the a-Si:H solar cell samples. The fitted values of the optical parameters are found to be in good agreement with published values.

The I-V characteristics curves of a-Si:H solar cells were measured. The parameters J_{sc}, V_{oc} , η and FF for the different samples, when the samples were illuminated with light of different intensities are determined and compared with published results. The paper presents the experimental results obtained from the transmittance spectra and the I-V characteristics measurements of the solar cell samples.

1. Introduction

Photovoltaic energy conversion refers to the direct conversion of the energy in light into usable electrical energy. Every fifteen minutes, the sun delivers enough radiant energy to the earth to meet mankind's power needs for a full year. The main goal of photovoltaics for large scale terrestrial applications is to harness this energy efficiently in a clean, convenient way at an affordable market cost. [1,17]

Solar cells represent the fundamental power conversion unit of a photovoltaic system. They are made from semiconductors and have much in common with other solid-state electronic devices, such as diodes, transistors and integrated circuits. Crystalline silicon cells hold the largest part of the market. [8]

To reduce the cost and make them competitive with other sources of energy, solar cells are assembled from materials of cheap cost such as amorphous silicon based alloys. Impressive progress in the research and use of amorphous silicon based alloys have been made since the results of the university of Dundee groups who demonstrated a low defect, device quality a-Si:H could be produced using radio frequency glow discharge in SiH_4 gas and that the material thus produced could be doped n- and p-type. The first single junction a-Si:H p-i-n solar cell, reported by Carlson and Wronski in 1976, had a conversion efficiency of 2.4 %. Large strides have been made in improving the conversion efficiency and at present the highest reported efficiency of such cells is 12.7 % [22]. This enormous improvement in the conversion efficiency is a result of a combination of a number of device and non-device related developments. The major device related developments include the use of a-SiC:H p-layer, superlattice doped layers, microcrystalline p-layers and microcrystalline n-layers. The non-device developments are related to optical enhancement features which include improvements in textured conductive transparent oxides such as indium-tin oxide (ITO) and tin oxide (SnO_2) and improvements in rear contacts with the use of titanium-silver alloys and

ITO-silver contacts. With recent reports of methods to improve open-circuit voltage one may expect an upper limit of 14 % on the conversion efficiency of single junction a-Si:H solar cells. The upper limit on the conversion efficiency of a-Si:H single junction cells is governed by the optical band gap of a-Si:H, which is 1.7 eV, and is not optimum for single junction terrestrial solar cells. The need to better utilise the solar spectrum, particularly in the long wavelength region has lead to great interest in developing a-Si based alloys with narrower band gaps than that of a-Si:H and to employ these materials in a stacked junction configuration. Moreover, better performance is expected from stacked junction cells with alloys of both wider (e.g., a-SiC:H) and narrower (e.g., a-SiGe:H) band gaps than that of a-Si:H. [3,16]

In this work, an attempt has been made to characterise the optical and electrical properties of a-Si:H solar cells. By simulating the measured transmittance spectra of a-Si:H pin solar cell samples quantities like the energy band gap, the layer thickness and the refractive indices of the different layer systems are determined. From the I-V characteristics measurement of a-Si:H solar cell samples the short circuit current, the open circuit voltage and the efficiency of the samples are determined.

In Section 2, basic physical concepts related to solar cells are discussed. The structure of amorphous silicon, preparation and growth of a-Si:H solar cells, the p-n and the p-i-n solar cell structures, the mobility and the energy band gap, the absorption and the transmittance are discussed. In addition, the I-V characteristics of a-Si:H solar cells, the factors that result to power losses and the effect of irradiance on the I-V characteristics of solar cells are considered.

The Forouhi and Bloomer dielectric function model and the SCOUTFIT computer program that are used to simulate the measured transmittance spectra of the solar cell samples are discussed in Section 3.

Section 4 is devoted to the discussion of the simulation of the transmittance spectra. The apparatus and the procedures used to measure the transmittance spectra are presented. The measured and the simulated transmittance spectra and the fitted values of the different optical parameters obtained from the simulation are displayed and compared with published values.

In Section 5, the apparatus and the experimental procedures related to the I-V characteristics measurements of the a-Si:H pin solar cell samples are presented. The results are tabulated, discussed and compared with published values.

Finally, in Section 6 concluding remarks are given and in Section 7 the reference materials are listed.

2. Optical and Electrical Properties of A-Si:H Solar Cells

Solar cells operate by converting sunlight into electricity using the electronic properties of a class of material known as semiconductors. In order to improve existing configurations, to choose materials and to understand the origins of the technical and economic problems of solar cells, one must have the knowledge of how these devices work. With these objectives in mind, a discussion of the optical and electrical properties of solar cells is presented in this section.

2. 1 Amorphous silicon

Amorphous semiconductors are disordered materials which contain large numbers of bonding and structural defects. They possess no long-range structural configuration which means there is no unit cell and no lattice. Rather, the semiconductor is composed everywhere of a random arrangement of ion cores which displays only short-range order. However, amorphous semiconductors, such as Si and Ge, can exhibit a high degree of short-range order. The nearest-neighbor separation in amorphous silicon (a-Si) is unchanged from the crystalline silicon (c-Si) to within 1 or 2 % [1].

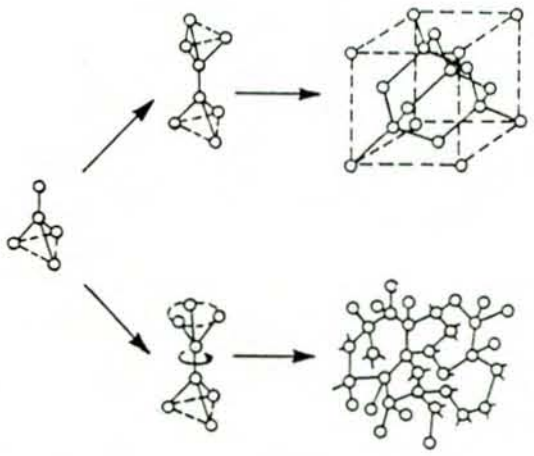

Figure 2. 1 The manner in which the basic tetrahedral unit can lead to a crystal or to an amorphous, random network material. [1]

Figure 2.1 shows how tetrahedral co-ordination leads to the face-centered-cubic unit cell of crystalline silicon and how tetrahedral structure can be preserved in the network model of amorphous silicon. Bonding defects as well as voids can be seen in this net work model of amorphous silicon.

Elemental amorphous silicon does not appear to possess any photovoltaic properties in itself. With out the constraints of periodicity, it is difficult for each silicon atom to be linked up with four others. This gives rise to microvoids within the structure of the material with unsatisfied (dangling) bonds. Combined with the nonperiodic arrangement of the atoms, this creates large densities of allowed states right across the normally forbidden band gap. These make it impossible to effectively "dope" the semiconductor or obtain reasonable carrier lifetimes.

However, it was reported in 1975 that amorphous silicon films produced by the glow discharge decomposition of silane (SiH_4) could be doped to form p-n junctions. These films contained hydrogen, created when the SiH_4 decomposes, as a reasonable proportion of the total atoms within the material (5 to 10 %). The role of hydrogen is to saturate the dangling bonds on the internal microvoids of the film and at other defects in the structure as shown in Figure 2.2. These would reduce the density of states within the forbidden gap and allow the material to be doped. [2]

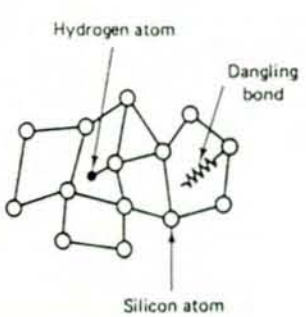

Figure 2. 2 Schematic diagram of the structure of amorphous silicon, showing how dangling bonds arise and how these may be passivated by hydrogen. [2]

2. 2 Preparation and growth of a-Si:H based alloys

Various techniques of depositing amorphous silicon based alloys have been attempted such as radio frequency (r.f.) glow discharge in SiH_4 gas, r.f. glow discharge in SiF_4 and H_2 gas mixtures, reactive sputtering of Si in H environment and chemical vapour deposition of SiH_4 gas. The major effort has concentrated on the first method, i.e., r.f. glow discharge in SiH_4 gas.

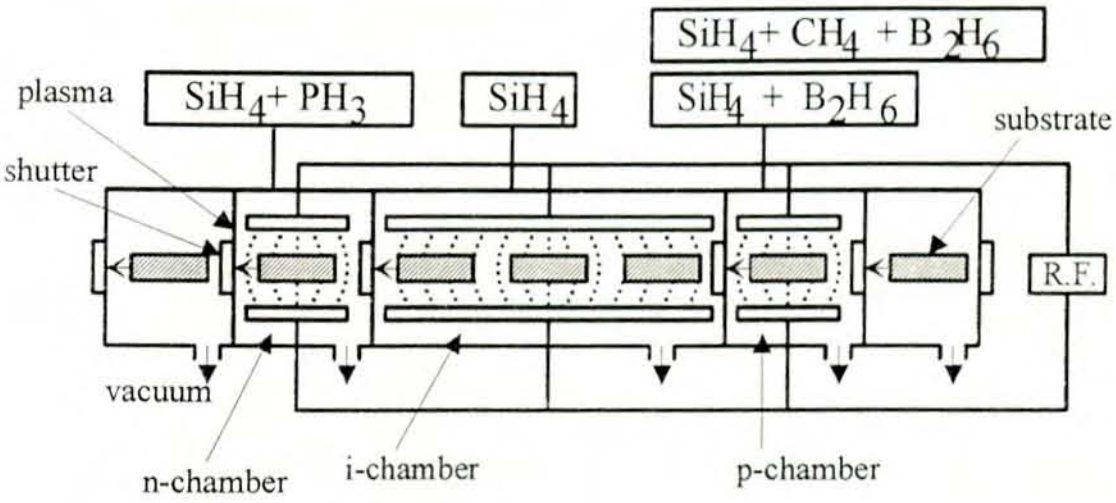

Figure 2. 3 Capacitively coupled glow discharge reaction system. [3]

A-Si films are generally prepared in a capacitively coupled system, as shown in Fig. 2.3. The gas is allowed to pass at a controlled rate between two plates and the plasma is generated between the plates using d.c., audio or r.f. frequencies. A variety of new species are produced, such as atoms, free radicals, stable and unstable ions. The energy of the electrons is on the order of a few electron volts (eV) and the electron temperature reached can be up to 100 times higher than that of the gas and hence the electron possesses enough energy to break down the molecular bonds. The electronic properties of the resultant a-Si based film depend on many deposition parameters such as temperature , gas flow rate, pressure, dilution, anode-cathode distance, power, etc. [3]

The present methods for improving a-Si:H appear to have three factors in common: (i) a reduction of the concentration of impurities such as O, C, and N, (ii) the avoidance of physical vapour deposition in favour of a surface deposition reaction by providing the proper siliconhydride radicals, and (iii) an increase of the deposition rate without sacrificing quality [4].

2. 3 p-n and p-i-n type solar cells

Various types of junction structures are developed for producing solar cells. The most common device structures are the p-n and the p-i-n. In crystalline semiconductors, such as c-Si, p-n junctions can be formed easily because of the high quality of the materials. A p-n junction crystalline silicon solar cell consists of a phosphorous doped n-layer deposited on a boron doped p-layer. To extract the photogenerated carriers (electrons and holes) to an external load, a front and a back metal contacts are deposited on the layers. Figure 2.4 shows a typical p-n junction solar cell.

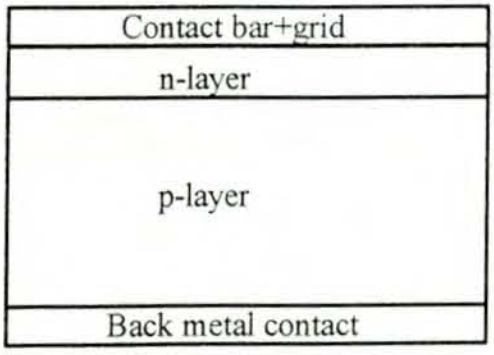

Figure 2. 4 A p-n junction solar cell structure.

The relatively poor transport properties in amorphous semiconductors, e.g. a-Si, necessities an additional intrinsic layer (i-layer) between the n- and p-layers. There are localised gap states, those arising out of unsatisfied chemical bonds and those arising out of structural defects and

impurities, which results to poor electrical properties in amorphous semiconductors. Dangling bonds inherent in semiconductors arise out of unsatisfied chemical bonds. Usually, hydrogen is added in a-Si to passivate the dangling bonds. The resulting semiconductor is referred to as hydrogenated amorphous silicon (a-Si:H). Hydrogen not only plays an important role in satisfying the dangling bonds but also modifies the whole structure of the semiconductor. It has been found that voids, usually present in conventional a-Si, tend to be absent in a-SiH_x [1]. The solar cells used in this work are made from a-Si:H.

The a-Si:H p-i-n solar cell consists of a glass substrate coated with TCO (transparent conducting oxide). A thin boron doped p-layer is deposited on the TCO which is followed by the i-layer and then a thin phosphorous doped n-layer. Finally, a back metal contact usually made of aluminium or silver is deposited on the n-layer. Figure 2.5 shows such a pin a-Si:H solar cell structure.

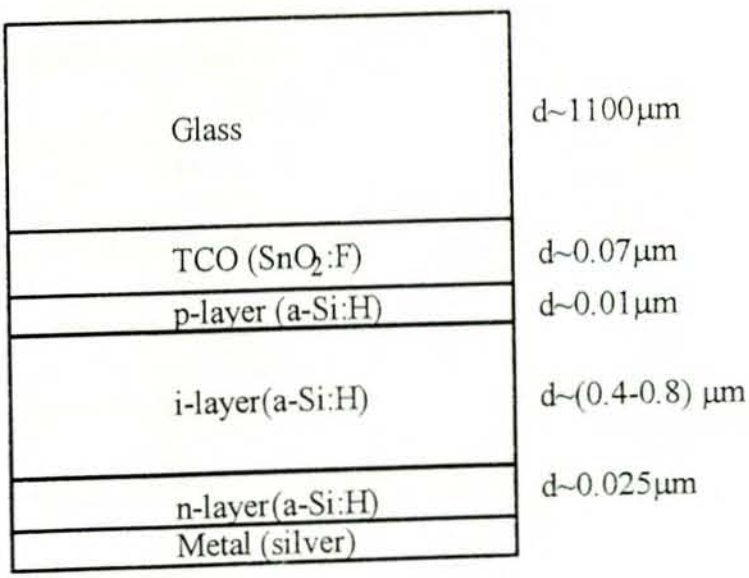

Figure 2. 5 A p-i-n junction solar cell structure.

2. 4 Mobilities and energy band gaps

Carriers transport in semiconductors is mainly by drift or diffusion, depending on whether the semiconductor is amorphous or crystalline. Consider a randomly moving electron in a crystal under the influence of an applied electric field, ξ. The electron collides with a lattice atom or an impurity or a defect in the crystal structure. The velocity that the electron gains from the applied field tends to decrease due to the collision process. For electrons in the conduction band, the average velocity increase between collisions caused by the field is given by

$$v_d = \frac{1}{2}\frac{e\tau}{m_e}\xi \tag{2.1}$$

where v_d is the drift velocity of the electron, τ is the relaxation time which is the average time between collisions, e is the elementary charge and m_e is the effective mass of the electron. If τ is averaged over all electron velocities, then Eqn. (2.1) becomes

$$v_d = \frac{e\tau}{m_e}\xi \tag{2.2}$$

The electron mobility (μ_e) is defined by

$$\mu_e = \frac{v_d}{\xi} = \frac{e\tau}{m_e} \tag{2.3}$$

and the current density (J_e) due to electrons in the conduction band is

$$J_e = env_d = e\mu_e n\xi \tag{2.4}$$

where n is the electron concentration.

Similarly, for holes in the valence band, the mobility (μ_h) is given by

$$\mu_h = \frac{e\tau}{m_h} \tag{2.5}$$

and the current density (J_h) is

$$J_h = e\mu_h p\xi \tag{2.6}$$

where m_h is the hole effective mass and p is the hole concentration.

The conductivity (σ) of the semiconductor is defined by

ADDIS ABABA UNIVERSITY LIBRARY

$$\sigma = \frac{J}{\xi} = e(\mu_e n + \mu_h p) \qquad (2.7)$$

The carrier mobility is affected by doping concentration and temperature. Doping a semiconductor heavily and increasing the temperature of the semiconductor results in a decrease of the carrier mobilities.

An electron in a crystal is found in a specified energy band. The energies of the valence electrons which form bonds between atoms represent the valence band. The next band with higher energy than the valence band is the conduction band. The forbidden energy gap that separates the valence band from the conduction band denotes the energy band gap (E_g). Energy band gaps are the characteristic of semiconductors and insulators. Semiconductors have energy gaps between 0.6 eV and 2.5 eV, whereas insulators have energy gaps which are greater than 2.5 eV. Being a semiconductor, the energy gap of c-Si is about 1.12 eV and that of a-Si is about 1.75 eV.

The major difference between c-Si and a-Si for solar cell application is in the energy band structure. Crystalline silicon possesses an indirect band gap structure whereas amorphous silicon possesses an almost direct band gap structure. The indirect band gap, in c-Si, necessities relatively thick devices (~100 μm). The mobilities of the holes and the electrons (μ_h~500 $cm^2/s.V$ and μ_e~1500 $cm^2/s.V$ [3]) in c-Si are large enough, so that light generated carriers are able to diffuse a p-n junction where they are transported to the contacts and hence generate a photocurrent. Hence, the main transport mechanism in crystalline silicon is diffusion. The direct band gap structure of a-Si allows to use relatively thin layers (~1 μm). The mobilities in a-Si are low (μ_e~10^{-1} $cm^2/s.V$ and μ_h~10^2 $cm^2/s.V$ [3]) and as a result the transport of photogenerated carriers is mainly through drift.

The optimum thickness of the different layer systems in solar cells depend not only on the mobility but also on the absorption coefficient. The next section is a discussion on the absorption.

2. 5 Absorption

Light incident on a semiconductor is attenuated as it passes through the semiconductor. The rate of absorption of light is proportional to the flux of photons for a given wavelength. The intensity of monochromatic light as it passes through the semiconductor is described mathematically as [2]

$$I(x) = I(x_0)e^{-\alpha(x-x_0)} \tag{2.8}$$

where α is the absorption coefficient. The absorption coefficient is important in solar cell design because it determines how far below the surface of the cell light of a given wavelength is absorbed and is used. Optical absorption is also used for characterising hydrogenated amorphous silicon (a-Si:H). Absorption coefficient for photon energies near the band gap are usually obtained from transmission and reflection measurements. [5]

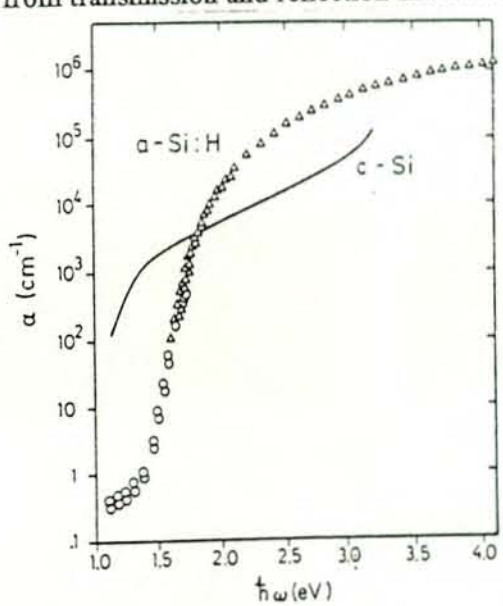

Figure 2. 6 Absorption coefficient of a-Si:H derived from optical absorption (Δ) and photoconductivity (O) [6].

Figure 2.6 shows the absorption edge obtained on a film of a-Si:H deposited at 240°C using optical absorption and photoconductivity. The Figure shows that a-Si:H is highly absorbing for photon energies greater than about 1.7 eV when compared with that of crystalline silicon.

2. 6 Transmittance

Suppose that a plane monochromatic wave having the form

$$\vec{E_i} = \vec{E_{oi}} \exp[i(\vec{k_i} \bullet \vec{r} - \omega t)] \tag{2.10}$$

is incident on an interface separating two isotropic media. Then, the reflected and the transmitted waves can be written as

$$\vec{E_r} = \vec{E_{or}} \exp[i(\vec{k_r} \bullet \vec{r} - \omega t)] \tag{2.11}$$

$$\vec{E_t} = \vec{E_{ot}} \exp[i(\vec{k_t} \bullet \vec{r} - \omega t)] \tag{2.12}$$

where $\vec{E}$ is the electric field, $\vec{k}$ is the wave vector, $\vec{r}$ is the position vector, ω is the frequency and t is the time.

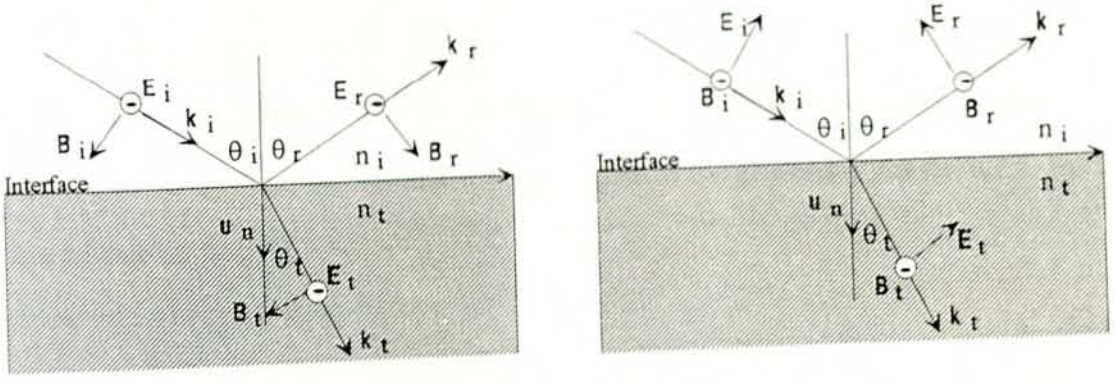

Figure 2. 7 An incoming wave whose electric field is (a) normal to the plane of incidence and (b) parallel to the plane of incidence.

An expression for the transmittance can be obtained by considering two cases: (i) when the electric field is perpendicular to the plane of incidence (s-polarisation) and (ii) when the electric field is parallel to the plane of incidence (p-polarisation).

s-polarisation

For s-polarisation it is assumed that $\vec{E}$ is perpendicular to the plane of incidence and $\vec{B}$ (the magnetic field) is parallel to it. Making use of the boundary conditions at the interface, i.e., from the continuity of the tangential components of the $\vec{E}$– and $\vec{B}$–fields, it is obtained that [7]

$$\left(\frac{E_\alpha}{Eoi}\right)_\perp = \frac{2\frac{n_i}{\mu_i}\cos\theta_i}{\frac{n_i}{\mu_i}\cos\theta_i+\frac{n_t}{\mu_t}\cos\theta_t} \tag{2.13}$$

Where n is the refractive index and μ is the permeability.

With dielectrics, for which $\mu_i \approx \mu_t \approx \mu_0$ equation (2.13) reduces to

$$t_\perp \equiv \left(\frac{E_\alpha}{Eoi}\right)_\perp = \frac{2n_i\cos\theta_i}{n_i\cos\theta_i+n_t\cos\theta_t} \tag{2.14}$$

where $t_\perp$ denotes the amplitude transmission coefficient for s-polarised light.

p-polarisation

In this case, it is assumed that $\vec{E}$ is parallel to the plane of incidence whereas $\vec{B}$ is perpendicular to it. From the continuity of the tangential components of the fields ($\vec{E}$ and $\vec{B}$), it can be derived that [7]

$$\left(\frac{E_\alpha}{E_{oi}}\right)_{//} = \frac{2\frac{n_i}{\mu_i}\cos\theta_i}{\frac{n_i}{\mu_i}\cos\theta_t+\frac{n_t}{\mu_t}\cos\theta_i} \tag{2.15}$$

When both media forming the interface are dielectrics, equation (2.15) becomes

$$t_{//} \equiv \left(\frac{E_\alpha}{E_{oi}}\right)_{//} = \frac{2n_i\cos\theta_i}{n_i\cos\theta_t+n_t\cos\theta_i} \tag{2.16}$$

where $t_{//}$ is the amplitude transmission coefficient in the case of p-polarisation.

The transmittance (T) is defined as the ratio of the intensity of the transmitted light to the intensity of the incident light. That is [7],

$$T = \frac{I_t \cos\theta_t}{I_i \cos\theta_i} = \frac{n_t \cos\theta_t}{n_i \cos\theta_i}\left(\frac{E_{ot}}{E_{oi}}\right)^2$$

$$\Rightarrow T = \left(\frac{n_t \cos\theta_t}{n_i \cos\theta_i}\right) t^2 \qquad (2.17)$$

where t is the amplitude transmission coefficient.

Thus, for s-polarised light

$$T_\perp = \left(\frac{n_t \cos\theta_t}{n_i \cos\theta_i}\right) t_\perp^2 \qquad (2.18)$$

and for p-polarised light,

$$T_{//} = \left(\frac{n_t \cos\theta_t}{n_i \cos\theta_i}\right) t_{//}^2 \qquad (2.19)$$

For normal incidence, i.e., for $\theta_i = 0$, the transmittance will be given by

$$T = T_\perp = T_{//} = \frac{4 n_t n_i}{(n_t + n_i)^2} \qquad (2.20)$$

2. 7 Current-Voltage (I-V) characteristics of solar cells

One of the methods used to characterise the performance of solar cells is to study the electrical properties of the solar cells. This is done by investigating the I-V characteristics curves of the solar cells. Figure 2.8 shows the band diagram of a p-n junction solar cell under illumination. Electron-hole pairs are generated on both sides of the junction. The p-n junction separates the minority carriers, electrons from the p-type base and holes from the n-type emitter, and transforms the light generated current between the bands into an electric current across the p-n junction.

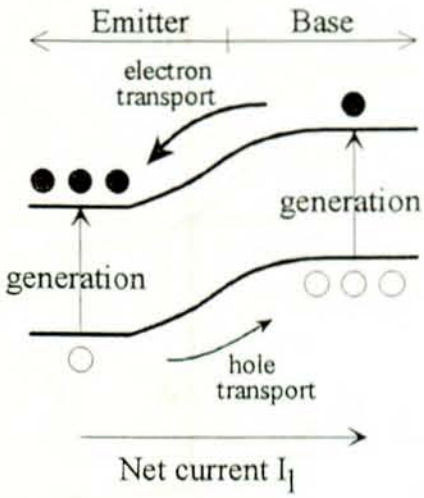

Figure 2. 8 Current in a p-n junction under illumination. [8]

The I-V characteristics of a solar cell can easily be understood by drawing an equivalent circuit of the device as shown in Figure 2.9a. The light generated current is represented by a current generator in parallel with a diode which represents the p-n junction [8]. The difference between the diode current (I_d) and the light generated current (I_l) is the output current (I) which is given by [7]

$$I = I_o\left(e^{\frac{eV}{mkT}} - 1\right) - I_l \tag{2.21}$$

where V is the voltage, k is the Boltzmann constant, e is the magnitude of the charge of an electron, T is the absolute temperature, I_o is the diode saturation current and m is the diode ideality factor whose value is usually close to unity.

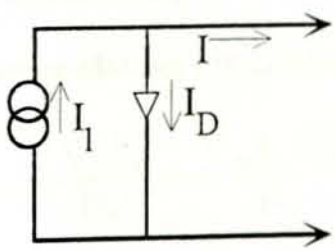

(a)

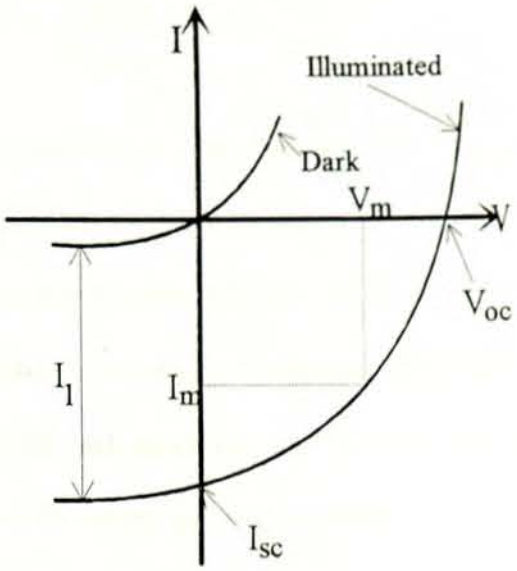

(b)

Figure 2. 9 The equivalent circuit (a) and the I-V characteristics of a solar cell (b). [2,8]

The current obtained when V = 0 is the short-circuit current (I_{sc}) and the voltage obtained when I = 0 is the open-circuit voltage (V_{oc}). An expression for V_{oc} can be obtained from Equation (2.21), by setting I = 0, as

$$V_{oc} = \frac{mkT}{e} \ln\left(\frac{I_l}{I_o} + 1\right) \tag{2.22}$$

The open-circuit voltage is determined by the properties of the semiconductor because of its dependence on I_o. The power output for any operating point in the fourth quadrant is equal to the area of the rectangle indicated in Figure 2.9b. The power output is maximum at the maximum power point (V_m , I_m), where V_m and I_m are the voltage and the current corresponding to the maximum power point respectively.

The energy conversion efficiency (η) of the solar cell is given by

$$\eta = \frac{V_m I_m}{P_{in}} = \frac{V_{oc} I_{sc} (FF)}{P_{in}} \tag{2.23}$$

where P_{in} is the total power of the light incident on the cell and FF is the fill factor, which is defined by the relation

$$FF = \frac{V_m I_m}{V_{oc} I_{sc}} \tag{2.24}$$

The fill factor is a measure of how "square" the output characteristics are. For cells of reasonable efficiency, it has a value in the range 0.70 to 0.85. [2]

The conversion efficiency of a practical solar cell is limited by intrinsic and extrinsic losses. The extrinsic losses include those due to reflection, series resistance, incomplete extraction of photogenerated carriers and recombination of carriers. The intrinsic loss includes the inability of a cell with a specific energy gap (E_g) to properly match the broad solar spectrum. These losses are discussed in the next section in more detail.

2. 8 Power losses in solar cells

Light incident on a solar cell creates electron-hole pairs. At the junction, the electrons and holes are made to separate by the intrinsic electric field and create a current flow in a load connected between the cell terminals. The main parameters that affect the energy-conversion efficiency of the cell are listed below together with the means to reduce the power losses.

- The light generated carriers have energy in excess of the band gap. Immediately after their formation, the electrons and holes decay to states near the edges of their respective bands. The excess energy is lost as heat. Moreover, the inability of semiconductors to absorb the below-band gap light causes a considerable part of the solar spectrum to be lost. These cases represent the fundamental loss mechanisms in solar cells.

  To reduce these losses, a tandem cell which represents a stack of several cells can be used. The top cell must be made of a wide-band gap semiconductor and it converts the more energetic (short wavelength) radiation. The transmitted light is then converted by the bottom cell which is made of a narrow-band gap semiconductor. This arrangement increases the efficiency, significantly.

- The maximum voltage that can be extracted from a solar cell is given by [8]

$$V = \frac{E_g}{e} \tag{2.25}$$

where E_g is the energy gap and e is the charge of an electron. Generally, a wide-band gap semiconductor produce higher voltage than a narrow-band gap semiconductor. However, the voltage obtained in practical devices is significantly less than to that expressed by Equation (2.25). The fundamental process that determines V_{oc} is recombination, which is the annihilation of electron-hole pairs, in the semiconductor. Recombination is most common at impurities and defects of the crystal or at the surface of the semiconductor. Recombination also takes place at the ohmic contacts with the semiconductor.

A layer of passivating oxide may be used to reduce surface recombination. The contacts can be surrounded by heavily-doped regions acting as "minority mirrors" which impede the minority carriers from reaching the contacts and recombining [8].

- Light reflection from the top surface, shading of the cell by the top contacts and incomplete absorption of light by semiconductors are also the other factors that result to power loss in solar cells.

Surface texturing and the application of two or more antireflection coating reduces the top surface reflection. Moving the top contacts to the back of the cell prevents the shading of the cell by the top contacts. By making the back metal contact optically reflecting, the absorption of light in solar cells can be improved.

- There are series and shunt resistances in solar cells that result to power losses. The series resistance (R_s) is due to the bulk resistance of the semiconductor making up the cell, the bulk resistance of the metallic contacts and interconnections and the contact resistance between the metallic contacts and the semiconductor.

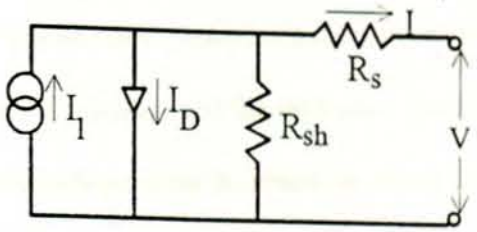

Figure 2. 10 An equivalent circuit of a solar cell [2].

The shunt resistance (R_{sh}) is caused by leakage across the p-n junction around the cell and in nonperipheral regions in the presence of crystal defects and precipitates of impurities in the junction region [2]. Both R_s and R_{sh} reduce the fill factor which in turn affects the output power. The effects of these resistances on the V_{oc}, the I_{sc} and the FF are shown in Figure 2.11.

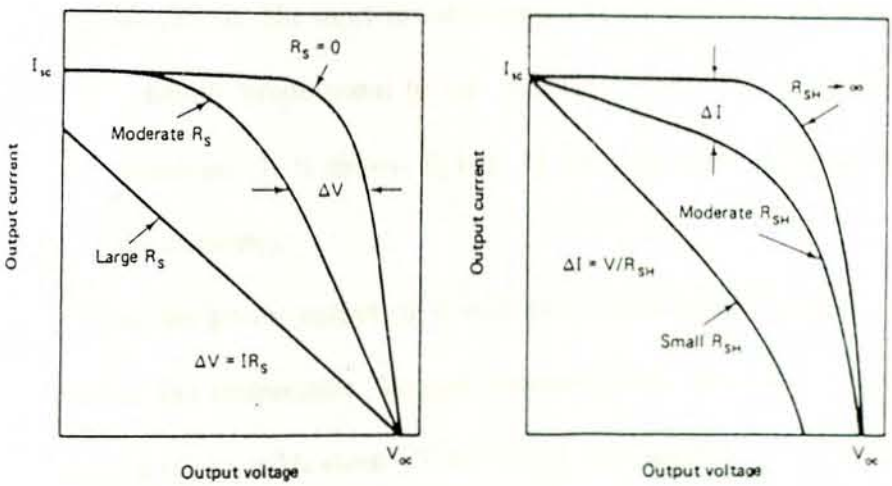

Figure 2. 11 Effects of R_s and R_{sh} on the I-V characteristics of solar cells. [2]

- The other factor that affects the power output of a-Si:H solar cells is the Staebler-Wronski effect. It is caused by the action of light absorption in the i-layer which create additional defects (photodegradation) by increasing the density of trappings

and scattering states, thereby reducing the efficiency of the solar cells. The Staebler-Wronski effect depends on the intensity of light to which the cell is exposed, the duration of the exposure and the thickness of the i-layer [8].

By using multiple-junction structure, in which the absorption of light is split between a number of relatively thin i-layers, the Staebler-Wronski effect can be reduced significantly. Increasing the amount of hydrogen also reduce the density of the dangling bonds which results to an increase in the efficiency of solar cells.

2. 9 Effects of irradiance and temperature on the I-V characteristics of solar cells

The total power from a radiant source falling on a unit area is known as irradiance [8]. When the irradiance is increased, the photon flux falling on the samples also increases resulting to a generation of a large current. The short-circuit current and the irradiance are related in such a way that the I_{sc} is directly proportional to the irradiance. The voltage dependence on the irradiance is not significant. It is shown in Eqn. (2.22) that open-circuit voltage depends logarithmically on the irradiance.

Temperature affects the power output of a solar cell. Most significantly, the open-circuit voltage depends on the temperature. Voltage decreases with increasing temperature. The voltage decrease of a silicon cell is about 2.3 mV/°C [2]. The short-circuit current of solar cells is not strongly dependent on temperature. It tends to increase slightly with increasing temperature. This is due to the fact that semiconductor band gaps generally decrease with temperature [2]. A decrease in band gap implies an increase of light absorption by the semiconductor.

3. Computer Simulation of the Transmittance Spectra of Multilayer Stacks

The simulation of the transmittance spectra of a-Si:H pin solar cell samples is performed using the SCOUTFIT computer program. The Forouhi and Bloomer (F&B) dielectric function model is also utilised in the simulation. A brief discussion on the F&B dielectric function model and the SCOUTFIT computer program is presented below.

3. 1 Forouhi and Bloomer dielectric function model

Optical properties of a medium can be described by the complex index of refraction, $N = n-i\kappa$ where n is the refractive index and κ is the extinction coefficient; or by the complex dielectric function, $\varepsilon = \varepsilon_1 - i\varepsilon_2$. ε is related to N by $\varepsilon = N^2$, so that $\varepsilon_1 = n^2 - \kappa^2$ and $\varepsilon_2 = 2n\kappa$. The parameters n and κ are referred to as optical constants of the medium. The optical constants depend on the photon energy, $E = \hbar\omega$, and exhibit structure in the interband region where bound-electron transitions are dominant. [9,10]

The extinction coefficient κ is directly related to the absorption coefficient α by

$$\kappa = \frac{\alpha c}{2\omega} \tag{3.1}$$

where c is the speed of light and ω is the frequency. A general expression for the extinction coefficient, κ, is obtained using the quantum-mechanical theory of absorption [9]. This expression is given by

$$\kappa(E) = \frac{A(E - E_g)^2}{E^2 - BE + C} \tag{3.2}$$

where,

$A = const.\frac{2\pi}{3}e^2\hbar^2|<\sigma^*|\mathbf{x}|\sigma>|^2\gamma,$

$B = 2(E_{\sigma^*} - E_\sigma),$

$C = (E_{\sigma^*} - E_\sigma)^2 + \frac{\hbar^2\gamma^2}{4},$

$|\sigma\rangle$ and $|\sigma^*\rangle$ are molecular states corresponding to energies E_σ and E_{σ^*}, $\mathbf{x}$ is the position vector, e is the charge of an electron $\hbar$ is Planck's constant and γ is the reciprocal of the life time of the excited state.

The optical constants n and κ are related by the Kramers-Kronig relation. Thus, an expression for n as a function of the energy (E) is given by [9]

$$n(E) = n(\infty) + \frac{B_0E + C_0}{E^2 - BE + C} \tag{3.3}$$

where ,

$B_0 = \frac{A}{Q}\left[-\frac{B^2}{2} + E_gB - E_g^2 + C\right],$

$C_0 = \frac{A}{Q}\left[(E_g^2 + C)\frac{B}{2} - 2E_gC\right],$

$Q = \frac{1}{2}(4C - B^2)^{\frac{1}{2}}$ and $n(\infty)$ is the refractive index at infinity.

It is shown that the five parameters, i.e., A, B, C, E_g and $n(\infty)$ describe the dependence of n and κ on the photon energy, E.

3. 2 SCOUTFIT computer simulation program

SCOUT is an abbreviation for SpectrosCopic Objects and UTilities and is a Windows application for Computer Assisted Optical Spectroscopy (CAOS). CAOS is an approach to the interpretation of optical spectra by computer simulation. [11]

A direct simulation of optical spectra has to be based on the macroscopic response of matter to electric fields which is given by the dielectric function of a material. Hence, the SCOUT provides a wide variety of possibilities to define dielectric functions, such as

- definition of dielectric function on the basis of models like the F&B model for interband transitions and the Drude model for free carriers.
- importing of dielectric function as a set of complex numbers, etc.

Transmittance and reflectance spectra can be analysed in SCOUTFIT program that comes with the SCOUT. SCOUTFIT is a computer program to fit model calculations of optical spectra automatically to experimental data. This is done by a variation of the unknown parameters and a comparison of the calculated to the measured spectra. If the parameter variation results in an improvement, the old parameters are replaced by the new ones. The parameter variation is continued until it is stopped by the user.

The SCOUTFIT's structure contains the main window which is a list of the fit parameters. The main window owns and controls the stack, the dielectric function and the spectra windows. The stack window defines the layer stack whose optical properties are to be fitted. The dielectric function window contains a list of the dielectric functions used by the SCOUTFIT. The spectra window is a list of the spectra used for the fit. The SCOUTFIT deals with one layer stack, but it can be made to fit simultaneously many spectra at a time. The parameters that can be fitted by the SCOUTFIT are layer thickness and dielectric functions.

In the SCOUTFIT program to prepare a parameter fit, it is necessary to define the dielectric functions of all materials to be used, the layer stack and the set up of the spectra that are to be compared to experimental data. After preparing the parameter list, the automatic fit is started. The performance of the fit requires a further refinement of the models until a complete automatic fit will be successful. The fitting process in the SCOUTFIT computer program is shown in Fig.3.1.

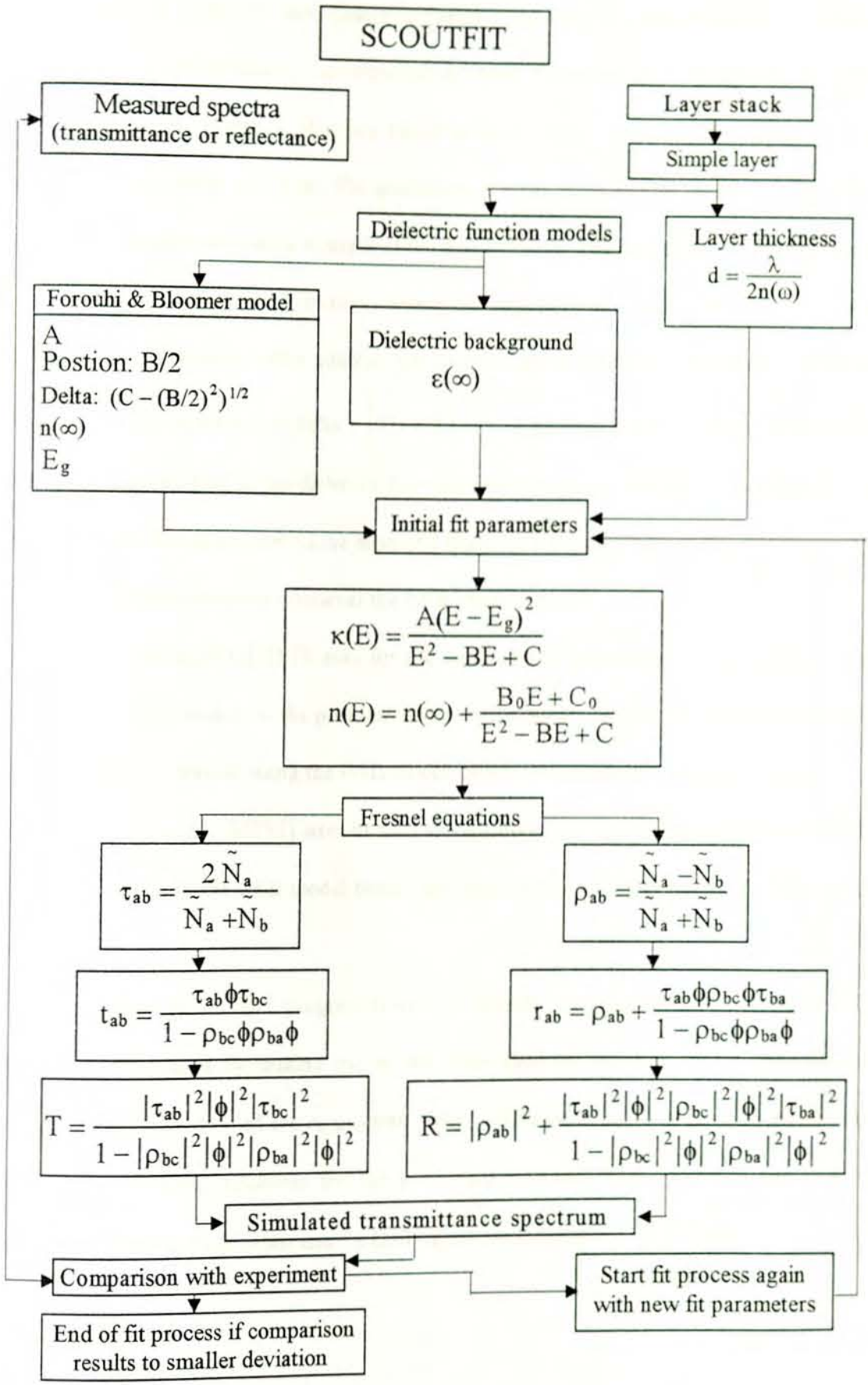

Figure 3. 1 The fitting process in the SCOUTFIT computer program.

The SCOUTFIT program uses dielectric function models, like the Forouhi and Bloomer model. For a fit of parameters to experiments, using the SCOUTFIT program, the original expressions for A, B and C that are found in Eqns. (3.2) and (3.3) are replaced by the parameters A, position and delta. The parameter A is the same as that found in Eqn. (3.2). It somewhat describes an overall strength of the susceptibility. The parameter position is equal to B/2 and it is the wavenumber position where the imaginary part of the dielectric function is maximum. The parameter delta controls the strength and at the same time acts as a damping parameter. Delta is defined as delta = $\left[C - \left(\frac{B}{2}\right)^2 \right]^{\frac{1}{2}}$. A positive choice of delta is not enough, since the imaginary part of the dielectric function can be negative if delta is too small [11]. It is known that the imaginary part of the dielectric function is always positive. So, it is necessary to check the dielectric function whenever the F&B model is used.

The F&B model in SCOUTFIT asks for the fundamental gap energy in wavenumbers. This wavenumber corresponds to the position where the imaginary part of the dielectric function is zero. The result of the fit, using the F&B model, below this wavenumber is not reliable.

The F&B model in SCOUTFIT uses its own extrapolation for high frequencies. Therefore, it is not advisable to use the F&B model beside any other susceptibility in the interband frequency region.

In this work the SCOUTFIT program is used to simulate the transmittance spectra of a-Si:H pin solar cell samples by making use of the F&B dielectric function model. The dielectric function parameters defined are A, position, delta, fundamental gap energy, refractive index at infinity and the layer thickness for the p-, i- and n-layers; layer thickness and dielectric background (real part) for glass and TCO (Transparent Conducting Oxide) layers.

4. Transmittance Spectra of A-Si:H Solar Cells

The transmittance measurement of solar cell samples is important for the optical characterisation of the samples. Section 4 is devoted to the presentation and discussion of the transmittance spectra of a-Si:H solar cell samples.

4. 1 Measuring the transmittance spectra

4. 1. 1 Measuring apparatus

The samples used in the transmittance measurements are two a-Si:H pin solar cells which differ in the i-layer thickness. The first one is denoted by TCOPIN1 and the second one by TCOPIN2 where TCO stands for transparent conducting oxide, P, I and N stand for boron doped a-Si:H p-layer, undoped a-Si:H intrinsic i-layer and phosphorous doped a-Si:H n-layer, respectively. The substrate is glass and the structure of the solar cells is of the type Glass/TCO/PIN/Ag where the back contact (i.e., silver) is absent on the spots where the transmittance is measured. The samples were produced by the glow-discharge method at the Juelich Research Center (Germany). The transmittance is measured on different spots of each samples. To differentiate the different spots on the samples the letters a, b and c are added in the samples notations. Thus, there are 6 spectra (3 for each sample) and are denoted by TCOPIN1a, TCOPIN1b, TCOPIN1c, TCOPIN2a, TCOPIN2b and TCOPIN2c.

The transmittance measurement of the samples were performed on a Perkin Elmers Lambda 19 UV/VIS/NIR double beam spectrometer. It measures the ratio of the intensity of the sample beam to the intensity of the reference beam. The Lambda 19, that is used for the transmittance measurement of the samples, consists of the main compartment of the spectrometer and the transmittance sample holder. It is used together with a personal computer. The optics of the Lambda 19 is shown in Figure 4.1.

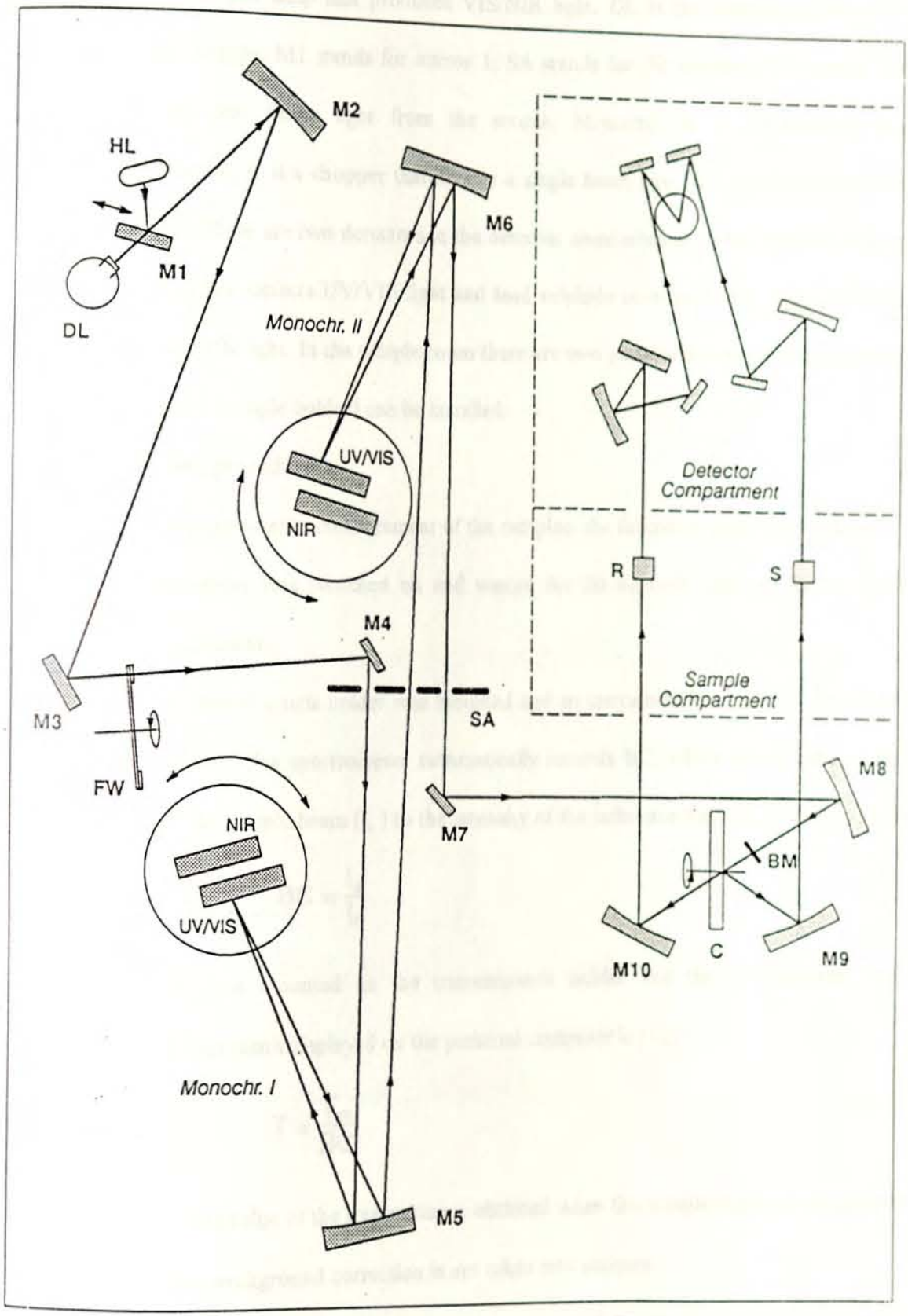

Figure 4. 1 Optics of Perkins Elmer Lambda 19 spectrometer. [14]

- HL is the halogen lamp that produces VIS/NIR light, DL is the deuterium lamp that produces UV light, M1 stands for mirror 1, SA stands for slit aperture, FW stands for filter wheel that filters light from the source, Monochr. is an abbreviation for monochromator, C is a chopper that divides a single beam into two and BM stands for beam mask. There are two detectors in the detector compartment room. Photomultiplier tube (PMT) that detects UV/VIS light and lead sulphide semiconductor (PbS) detector that detects NIR light. In the sample room there are two parts where R (reference mirror holder) and S (sample holder) can be installed.

4. 1. 2 **Measuring procedures**

When taking the transmittance measurement of the samples, the following steps were taken:

- The spectrometer was switched on and waited for 20 minutes until the lamps reach thermal equilibrium.
- The transmittance sample holder was mounted and an instrument background correction (BC) was done. The spectrometer automatically records BC, which is the ratio of the intensity of the sample beam (I_s) to the intensity of the reference beam (I_r). That is [12],

$$BC = \frac{I_s}{I_r} \tag{4.1}$$

- The sample was mounted on the transmittance holder and the measurement was performed. The result displayed on the personal computer is [12]

$$T = \frac{T_m}{BC} \tag{4.2}$$

where T_m is the value of the transmittance obtained when the sample is put on the sample holder so that background correction is not taken into account.

- The measured transmittance spectra were converted to an xy-format, where the wavelength which was measured in nanometers (nm) is converted to wavenumbers in

units of cm^{-1}, using the Origin 4.0 computer program. The measured spectra in units of cm^{-1} were simulated using the SCOUTFIT computer program to obtain the fitted curves for each spectra.

- The fitted values of the dielectric background (real part) and the layer thickness for glass and TCO layers; refractive index at infinity, layer thickness, energy gap and the parameters A, position and delta of the p-, i- and n-layers were obtained from the SCOUTFIT computer fitting process. The fitted values that are tabulated in sections 4.2.1 and 4.2.2 were taken when the χ^2 deviation (see below) was as small as possible.

Chi squared (χ^2)

The results of any repeated measurement can be grouped in bins (a number of intervals), k=1,...,n. Let O_k denote the number of results observed in bin k. Similarly, E_k denote the number expected in bin k, based on some assumed distribution. Chi squared is defined as

$$\chi^2 = \sum_{k=1}^{n} \frac{(O_k - E_k)^2}{E_k} \tag{4.3}$$

and the reduced chi squared as

$$\tilde{\chi} = \frac{\chi^2}{d} \tag{4.4}$$

where d is the number of degrees of freedom. If $\tilde{\chi} >> 1$, the agreement between O_k and E_k is bad and the assumed distribution is rejected. If $\tilde{\chi} \leq 1$, the agreement is satisfactory, and the observed and expected distributions are compatible. [13]

4. 2 Measured and simulated transmittance spectra (results and discussion)

The simulation of the transmittance spectra is done by using the SCOUTFIT computer program, in the wavenumbers interval between 12000 cm^{-1} and 20000 cm^{-1} (i.e., in the energy range between 1.49 eV and 2.48 eV). The dielectric function model used in the simulation is the Forouhi and Bloomer model. The experimental and the simulated spectra are presented and discussed below.

4. 2 .1 Measured and simulated transmittance spectra of the TCOPIN1 sample

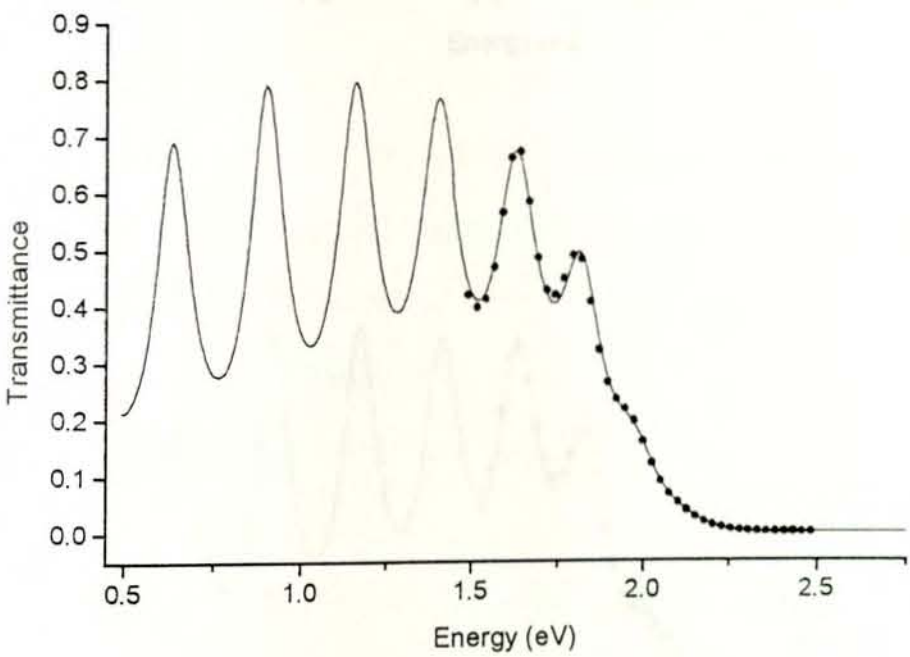

(a)

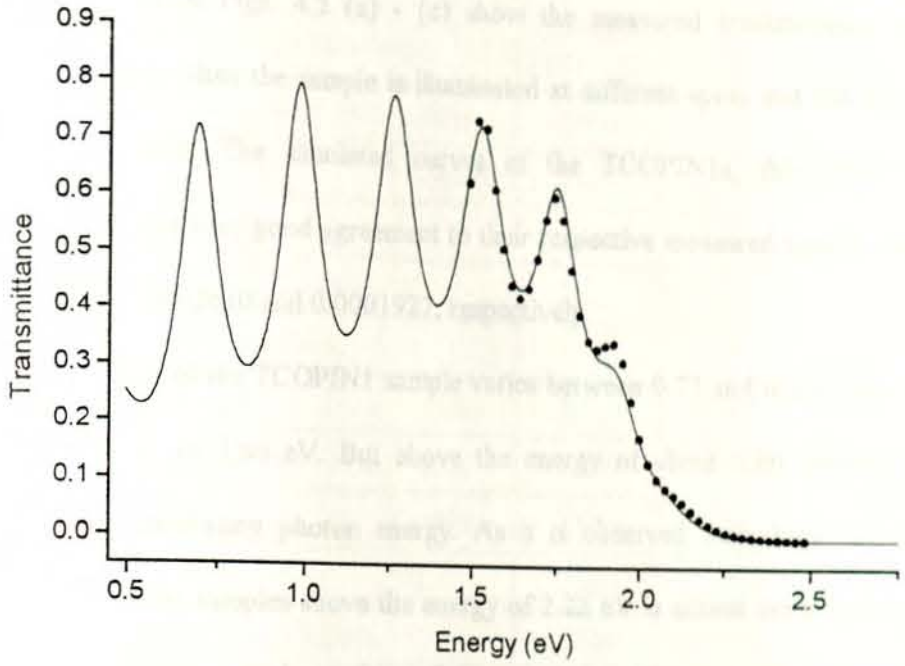

(b)

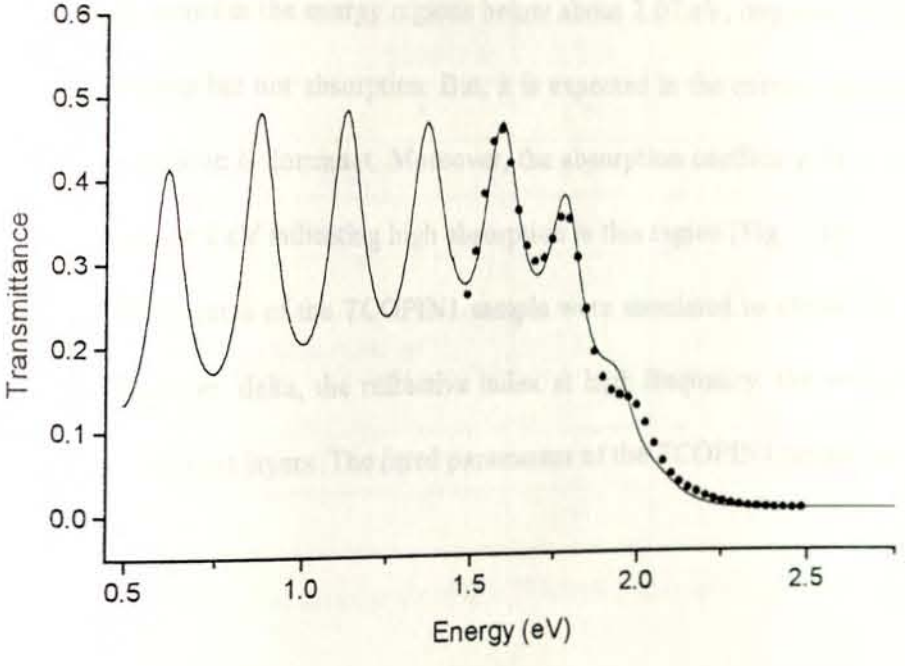

(c)

Figure 4. 2 The measured (solid) and the simulated (dotted) transmittance spectra curves of the (a) TCOPIN1a, (b) TCOPIN1b and (c) TCOPIN1c.

The solid curves of Figs. 4.2 (a) - (c) show the measured transmittance spectra of the TCOPIN1 sample when the sample is illuminated at different spots and the dotted curves are the simulated ones. The simulated curves of the TCOPIN1a, the TCOPIN1b and the TCOPIN1c are in a very good agreement to their respective measured spectra with a deviation of 0.0000782, 0.0002610 and 0.0001927, respectively.

The transmittance of the TCOPIN1 sample varies between 0.73 and 0.28 in the energy region between 1.49 eV to 1.86 eV. But above the energy of about 1.86 eV, the transmittance decreases with increasing photon energy. As it is observed from Figs. 4.2 (a) - (c), the transmittance of the samples above the energy of 2.22 eV is almost zero. In this region either there is high reflection at the surface of the samples or else there is high absorption in the layers. But, above about 600 nm (i.e., below 2.07 eV) a-Si:H no longer absorbs essentially all the light [15]. It means in the energy regions below about 2.07 eV, one may observe reflection and (or) transmission but not absorption. But, it is expected in the energy regions above about 2.07 eV that absorption is dominant. Moreover, the absorption coefficient of a-Si:H is high for energies above about 2 eV indicating high absorption in this region [Fig. 2.2].

The transmittance spectra of the TCOPIN1 sample were simulated to obtain the values of the parameters A, position, delta, the refractive index at high frequency, the energy gap and the thickness of the different layers. The fitted parameters of the TCOPIN1 sample are displayed in Table 4.1.

Layer systems	Optical parameters	Fitted values			Dim.
		TCOPIN1a	TCOPIN1b	TCOPIN1c	
N-layer	Forouhi & Bloomer (1986) : delta	1.429	1.297	1.245	eV
"	" : position	2.433	2.461	3.228	eV
"	" : A	1.568	1.568	1.566	-
"	Refractive index at infinity	3.385	3.401	3.431	-
"	Fundamental gap energy	1.727	1.724	1.723	eV
"	Layer thickness	0.025	0.022	0.026	μm
I-layer	Forouhi & Bloomer (1986) : delta	1.209	1.398	1.366	eV
"	" : position	2.505	2.386	2.059	eV
"	" : A	1.563	1.564	1.57	-
"	Refractive index at infinity	2.396	2.382	2.387	-
"	Fundamental gap energy	1.653	1.653	1.653	eV
"	Layer thickness	0.502	0.48	0.483	μm
P-layer	Forouhi & Bloomer (1986) : delta	1.416	1.516	1.414	eV
"	" : position	3.131	3.157	3.056	eV
"	" : A	1.56	1.57	1.564	-
"	Refractive index at infinity	3.43	3.415	3.36	-
"	Fundamental gap energy	1.926	1.925	1.925	eV
"	Layer thickness	0.009	0.01	0.009	μm
TCO	Dielectric background (real part)	3.831	3.727	3.829	-
"	Layer thickness	0.07	0.077	0.068	μm
Glass	Dielectric background (real part)	2.269	2.272	2.264	-
"	Layer thickness	1116	1115	1101	μm

Table 4. 1 The fitted optical parameters of the TCOPIN1 sample. (Dim. stands for dimension)

Table 4.1 shows that the deviation of the different optical parameters from each other of the transmittance spectra of the TCOPIN1 sample taken at different spots of the sample is small, indicating that the fitted optical parameters characterise the given sample effectively. In relative terms, the deviation from each other of the thickness of the sample at the different spots is

large. This may be accounted for the inhomogeneity of the thickness of the layers during the preparation of the samples.

4. 2. 2 Measured and simulated transmittance spectra of the TCOPIN2 sample

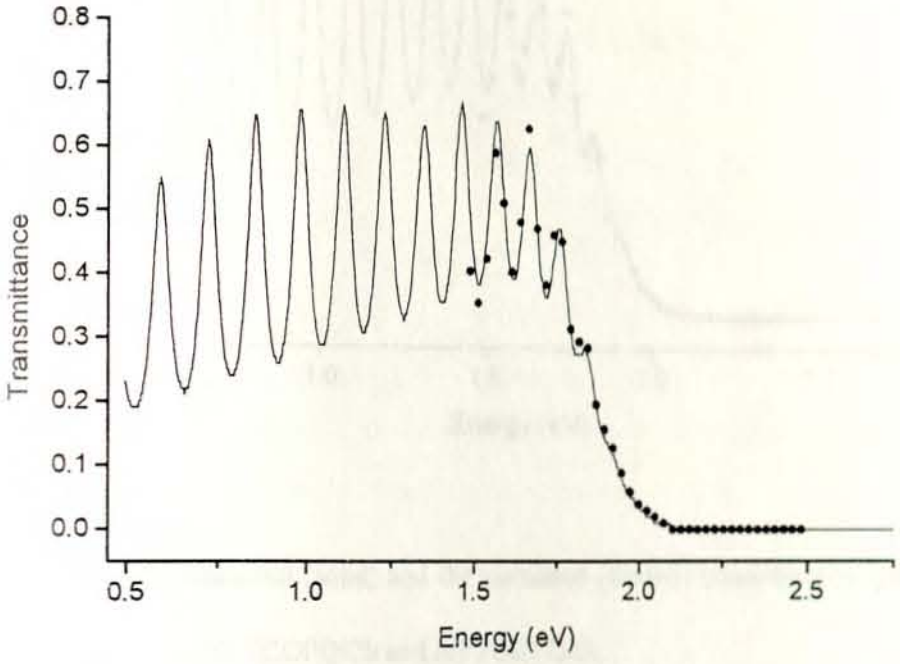

(a)

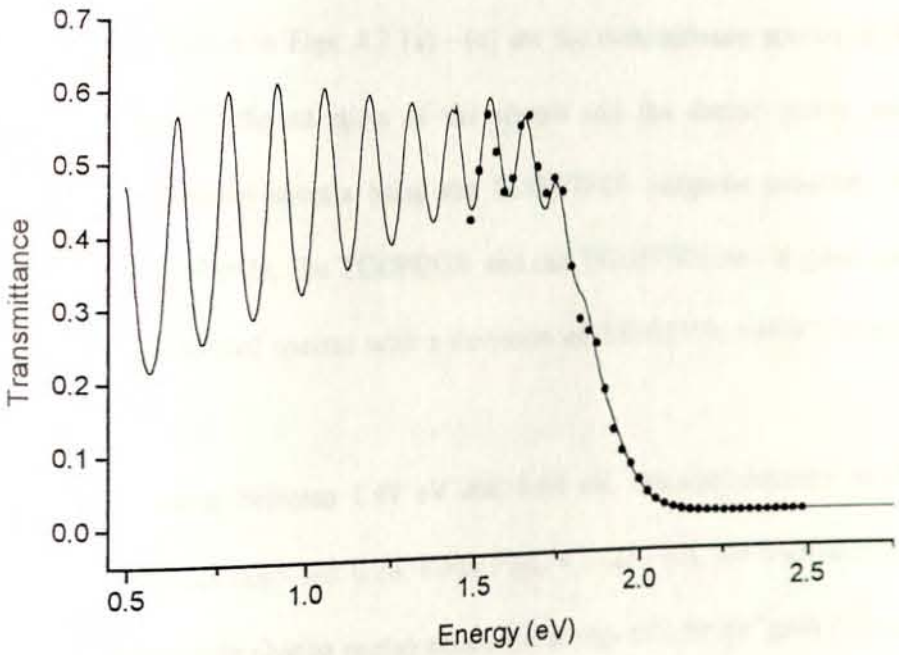

(b)

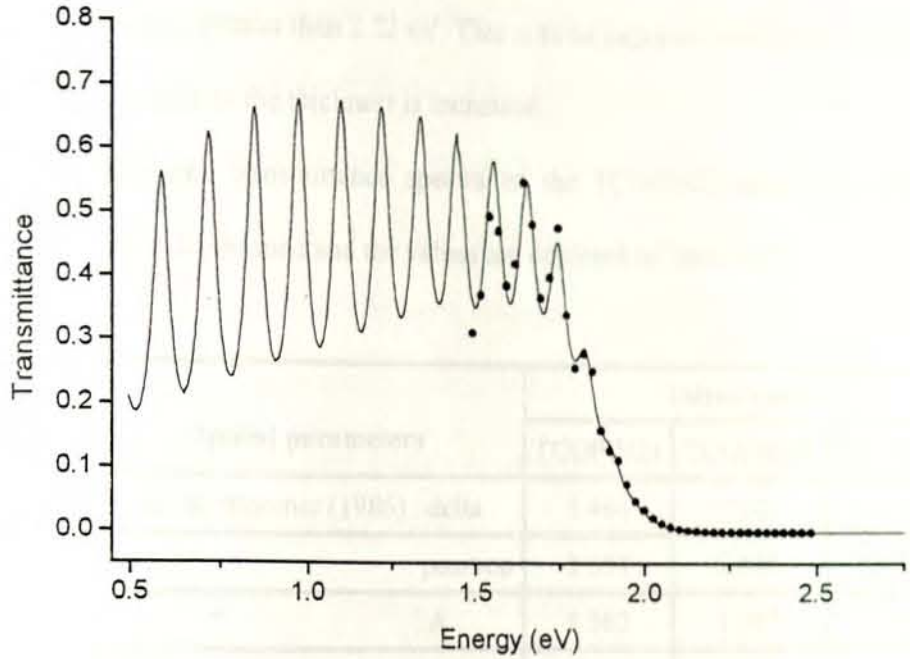

(c)

Figure 4. 3 The measured (solid) and the simulated (dotted) transmittance spectra curves of the (a) TCOPIN2a, (b) TCOPIN2b and (c) TCOPIN2c.

The solid curves shown in Figs. 4.3 (a) - (c) are the transmittance spectra of the TCOPIN2 sample measured at different spots of the sample and the dotted curves are obtained by simulating the measured spectra using the SCOUTFIT computer program. The simulated spectra of the TCOPIN2a, the TCOPIN2b and the TCOPIN2c are in good agreement with their respective measured spectra with a deviation of 0.0003759, 0.0002871 and 0.0003081, respectively.

In the energy interval between 1.49 eV and 1.84 eV, the transmittance of the TCOPIN2 sample varies between 0.65 and 0.26. From Figs. 4.3 (a) - (c), the transmittance is found to decrease with increasing photon energy above the energy of 1.84 eV, until it is almost zero for energy greater than about 2.07 eV. The transmittance of the TCOPIN2 sample approaches zero faster than that of the TCOPIN1. That is, for the TCOPIN2 sample the transmittance approaches zero for energy greater than 2.07 eV, whereas for the TCOPIN1 it approaches

zero for the energy greater than 2.22 eV. This is to be expected since the absorption of light in a material increases as the thickness is increased.

From the simulated transmittance spectra of the TCOPIN2 sample the different optical parameters were determined and the values are depicted in Table 4.2.

Layer systems	Optical parameters	Fitted values			Dim.
		TCOPIN2a	TCOPIN2b	TCOPIN2c	
N-layer	Forouhi & Bloomer (1986) : delta	1.466	1.142	1.185	eV
"	" : position	3.054	2.485	2.917	eV
"	" : A	1.567	1.565	1.568	-
"	Refractive index at infinity	3.414	3.41	3.403	-
"	Fundamental gap energy	1.723	1.723	1.722	eV
"	Layer thickness	0.025	0.028	0.025	µm
I-layer	Forouhi & Bloomer (1986) : delta	1.183	1.193	1.226	eV
"	" : position	2.607	2.277	2.455	eV
"	" : A	1.668	1.57	1.569	-
"	Refractive index at infinity	2.44	2.417	2.335	-
"	Fundamental gap energy	1.65	1.653	1.652	eV
"	Layer thickness	1.031	0.863	1.054	µm
P-layer	Forouhi & Bloomer (1986) : delta	1.509	1.459	1.342	eV
"	" : position	2.72	2.634	3.064	eV
"	" : A	1.569	1.567	1.566	-
"	Refractive index at infinity	3.41	3.4	3.411	-
"	Fundamental gap energy	1.926	1.927	1.926	eV
"	Layer thickness	0.01	0.009	0.01	µm
TCO	Dielectric background (real part)	3.811	3.961	3.83	-
"	Layer thickness	0.066	0.072	0.077	µm
Glass	Dielectric background (real part)	2.247	2.27	2.233	-
"	Layer thickness	1106	1100	1093	µm

Table 4. 2 The fitted optical parameters of the TCOPIN2 sample.

Similar to the TCOPIN1 sample, the deviation of the optical parameters of the TCOPIN2 sample from each other for the different sample spots is small. This seems to indicate that the fitted optical parameters successfully characterise the given sample. Here also, relatively big deviation is observed in the layer thickness for the different spots, which indicates the difficulty encountered in depositing the a-Si:H layers homogeneously on the substrate.

It is observed from the transmittance spectra of the TCOPIN1 and the TCOPIN2 samples that the separation between any two maxima or minima (i.e., the broadness of the interference fringes) is different for the samples. The cause for the difference in the broadness of the fringes is the difference in the i-layer thickness of the samples. The interference fringes (the spectra) are observed due to the interaction of light with the different layers that make up the solar cells. The broadness of the fringes is a function of the layer thickness. They are related in such a way that as the thickness of the layers is increased, the broadness of the interference fringes decreased and vice versa.

The difference in the simulated layer thickness of both the TCOPIN1 and the TCOPIN2 samples at different spots indicates that the different layers are deposited on the substrate inhomogeneously. In fact, it is mainly this inhomogeneity that results to the different transmittance spectra of the samples when measured at different spots on the same samples.

4. 3 Comparison of results

The average values of the fitted optical parameters of the TCOPIN1 and the TCOPIN2 samples are calculated and compared with reference values in order to determine the percentage deviation. Tables 4.3 and 4.4 show these comparisons.

Layer systems	Optical parameters	Fitted average values	Reference values	Deviation (%)	Dim.
N-layer	Forouhi & Bloomer (1986) : delta	1.324	1.41 [9]	6.02	eV
"	" : position	2.707	2.767 [9]	2.17	eV
"	" : A	1.567	1.569 [9]	0.13	-
"	Refractive index at infinity	3.406	3.42 [18]	0.41	-
"	Fundamental gap energy	1.725	1.723 [9]	0.12	eV
"	Layer thickness	0.024	0.025 [19]	4	μm
I-layer	Forouhi & Bloomer (1986) : delta	1.324	1.41 [9]	6.02	eV
"	" : position	2.317	2.767 [9]	16.26	eV
"	" : A	1.567	1.569 [9]	0.13	-
"	Refractive index at infinity	2.388	2.43 [10]	1.85	-
"	Fundamental gap energy	1.653	1.653 [9]	0	eV
"	Layer thickness	0.488	0.455 [19]	7.25	μm
P-layer	Forouhi & Bloomer (1986) : delta	1.449	1.41 [9]	2.77	eV
"	" : position	3.114	2.767 [9]	12.54	eV
"	" : A	1.565	1.569 [9]	0.26	-
"	Refractive index at infinity	3.402	3.42 [18]	0.53	-
"	Fundamental gap energy	1.925	1.925 [9]	0	eV
"	Layer thickness	0.009	0.01 [19]	10	μm
TCO	Dielectric background (real part)	3.797	3.8 [20]	0.08	-
"	Layer thickness	0.072	0.07 [19]	2.86	μm
Glass	Dielectric background (real part)	2.268	2.25 [20]	0.8	-
"	Layer thickness	1111	1100 [21]	1	μm

Table 4. 3 The fitted average values of the optical parameters of the TCOPIN1 sample.

From Table 4.3 it is observed that the deviations of the parameters delta and position are relatively large for the different layer systems. These deviations may have resulted because of the difference in the solar cells quality. That is, since 1986 when the parameters A, position and delta were first determined for a-Si:H [9], significant improvements have been made in the design and fabrication of solar cells. Hence, the improvement in the solar cells quality may result to a change in the above mentioned parameters, which may in turn contribute to the observed deviations from the reference values.

On the other hand, the deviations in the energy gaps and the refractive indices from the reference values are small. These suggest that the dielectric function model that is used for the simulation is effective in determining the given optical parameters.

It is observed during the fitting process that, for the n-layer, by changing (i.e., decreasing or increasing) the values of the parameter position and the layer thickness; the chi squared deviation could be kept constant. Similarly, for the i-layer keeping the deviation constant, the energy band gap (E_g) could be adjusted by changing the parameter delta. Hence, knowing the values of the parameters A, position and delta accurately lead to an accurate determination of the energy gaps (E_g), the refractive indices at high frequency and the layer thickness of the different layers of a-Si:H p-i-n solar cell samples.

Layer systems	Optical parameters	Fitted average values	Reference values	Deviation (%)	Dim.
N-layer	Forouhi & Bloomer (1986) : delta	1.264	1.41 [9]	10.36	eV
"	" : position	2.819	2.767 [9]	1.88	eV
"	" : A	1.567	1.569 [9]	0.13	-
"	Refractive index at infinity	3.409	3.42 [18]	0.32	-
"	Fundamental gap energy	1.723	1.723 [9]	0	eV
"	Layer thickness	0.026	0.025 [19]	4	μm
I-layer	Forouhi & Bloomer (1986) : delta	1.201	1.41 [9]	14.11	eV
"	" : position	2.446	2.767 [9]	11.6	eV
"	" : A	1.602	1.569 [9]	2.1	-
"	Refractive index at infinity	2.397	2.43 [10]	1.48	-
"	Fundamental gap energy	1.652	1.653 [9]	0.06	eV
"	Layer thickness	0.983	0.875 [19]	14.29	μm
P-layer	Forouhi & Bloomer (1986) : delta	1.437	1.41 [9]	1.92	eV
"	" : position	2.806	2.767 [9]	1.41	eV
"	" : A	1.567	1.569 [9]	0.13	-
"	Refractive index at infinity	3.407	3.42 [18]	0.38	-
"	Fundamental gap energy	1.926	1.925 [9]	0.05	eV
"	Layer thickness	0.01	0.01 [19]	0	μm
TCO	Dielectric background (real part)	3.867	3.8 [20]	1.76	-
"	Layer thickness	0.072	0.07 [19]	2.86	μm
Glass	Dielectric background (real part)	2.25	2.25 [20]	0	-
"	Layer thickness	1100	1100 [21]	0	μm

Table 4. 4 The fitted average values of the optical parameters of the TCOPIN2 sample.

Table 4.4 shows that the deviations of the parameters delta and position, specially for n- and i-layers, are relatively large. These deviations from the reference values may be due to the difference in the quality of the a-Si:H layers. Similar to the TCOPIN1 sample, the deviations of the energy gaps and the refractive indices of the TCOPIN2 sample from the reference values

are small. These may tell us about the effectiveness of the Forouhi and Bloomer dielectric function model in determining the given optical parameters.

Knowing the energy gaps of the different layer systems is important in the design of solar cells. A-Si:H p-i-n solar cells must be designed in such a way that the p-layer has a wide energy gap compared to that of the i- and n-layers, in order to reduce light absorption in the front layer. The fitted average values of the energy gap of the p-, i- and n-layers are 1.925 eV, 1.653 eV and 1.725 eV for the TCOPIN1; 1.926 eV, 1.652 eV and 1.723 eV for the TCOPIN2, respectively. Most of the incident light flux having energy less than 1.925 eV will pass the p-layer without being absorbed. In a-Si:H solar cells, the active layer where electron-hole pairs are desired to be created is the i-layer. Thus, the i-layer absorbs most of the flux of photons that escape the front layers. It is mainly the electron-hole pairs that are formed in the i-layer which are responsible for the output current that is obtained from a-Si:H solar cells.

Finally, it can be concluded that the Forouhi and Bloomer dielectric function model is effective in determining the energy gap, the refractive index at high frequency and the layer thickness of the different layer systems of a-Si:H p-i-n solar cell samples.

The simulation of the transmittance spectra is more successful for the TCOPIN1 sample than that for the TCOPIN2. It is known that the difference between the two samples is in their i-layer thickness. It means, the Forouhi and Bloomer dielectric function model is more effective for thin layers than thick layers. Extending this argument, one may conclude that the model is more effective to characterise individual layers rather than a stack of layers.

4. 4 Dielectric function of the n-layer

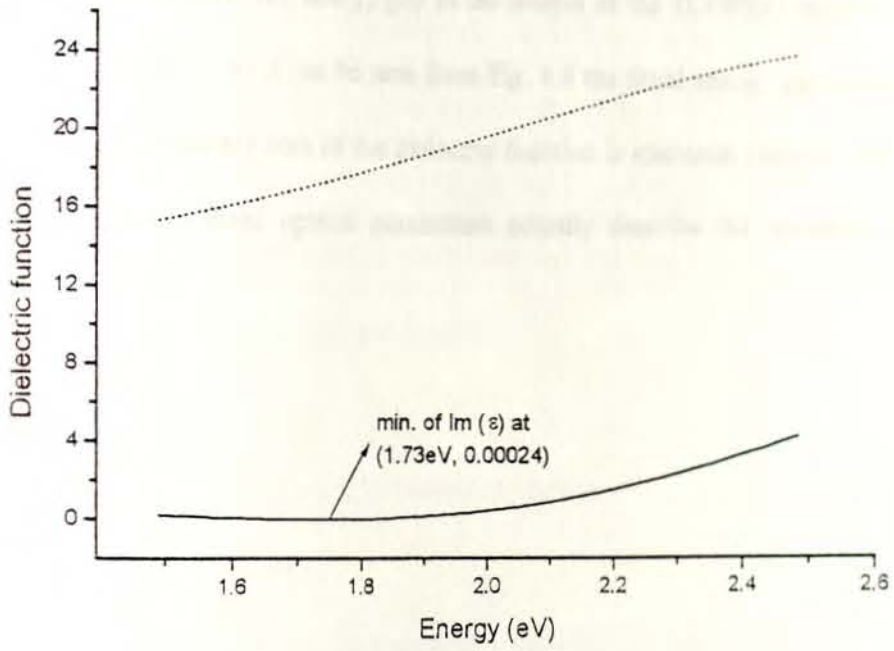

Figure 4. 4 The simulated dielectric function of the n-layer of the TCOPIN1 sample (The solid curve is the imaginary part and the dashed curve is the real part).

The dielectric function of the n-layer of the TCOPIN1 sample is shown in Figure 4.4. It is seen from the graph that the real part of the dielectric function (ε_1) increases with increasing energy. The imaginary part of the dielectric function (ε_2) decreases between the energy range of about 1.49 eV and 1.73 eV. It becomes almost zero between about 1.69 eV and 1.78 eV and increases with increasing energy beyond the energy of about 1.73 eV. The refractive index (n) of the n-layer increases with increasing energy even when ε_2 is zero. From Eqn. (3.1), it is shown that the absorption is directly proportional to the extinction coefficient (κ). In the regions where the energy is between 1.69 eV and 1.78 eV, ε_2 is almost zero which implies that κ is also practically zero. This in turn implies that there is no absorption of light in the n-layer in the given energy region.

The Forouhi and Bloomer dielectric function model in SCOUTFIT defines the energy gap in wavenumbers. This is the wavenumber position where the imaginary part of the dielectric function is smallest [11]. The energy gap of the n-layer of the TCOPIN1 sample is found to be 1.73 eV (13901 cm^{-1}). As it can be seen from Fig. 4.4 the fitted energy gap corresponds to the point where the imaginary part of the dielectric function is minimum (almost zero). This seems to confirm that the fitted optical parameters actually describe the measured transmittance spectra.

5. I-V Characteristics of A-Si:H Solar Cells

The I-V characteristics measurement of solar cells is important to characterise the performance of the solar cells. From the I-V characteristics curves it is possible to determine quantities like the short circuit current density (J_{sc}), the open circuit voltage (V_{oc}), the Fill factor (FF) and the efficiency (η) of different types of solar cells. In this section the apparatus and the method used to determine the I-V characteristics curves and the different solar cell parameters obtained from the I-V curves are presented and discussed.

5. 1 Measuring the I-V characteristics curves

5. 1. 1 Measuring apparatus

The devices used for the I-V characteristics measurement are a 250 W stabilised quartz tungsten halogen lamp, two digital multimeters (one for current measurement and the other for voltage measurement), variable load (rheostat), a calibrated Lux meter which uses a silicon photodiode, two lenses (with $f_1 = +150$ mm and $f_2 = -100$ mm), a-Si:H samples and a personal computer to analyse the measured data.

5. 1. 2 Measuring Procedures

The I-V characteristics measurement was performed on two a-Si:H solar cell samples. The samples are the TCOPIN1 and the TCOPIN2 which differ only in the i-layer thickness (the i-layer thickness of the TCOPIN1 is about 488 nm and that of the TCOPIN2 is about 983 nm). When taking measurements of the I-V characteristics of the samples the following steps were taken.

- The apparatus was arranged as it is shown in Figure 5.1.
- The lamp was set on and the samples were illuminated with light of the required intensity (10, 50 or 100 $mWcm^{-2}$). The intensity was measured with the Lux meter at the point where the samples are located.

5. 2 J-V characteristics of a-Si:H solar cells (results & discussion)

The J-V characteristics of the TCOPIN1 and the TCOPIN2 samples when they are illuminated with light of different intensities are shown below. The V_{oc} , the J_{sc} , the η and the FF for the different intensities of white light illumination are determined and the values are given in the tables that accompany the respective curves.

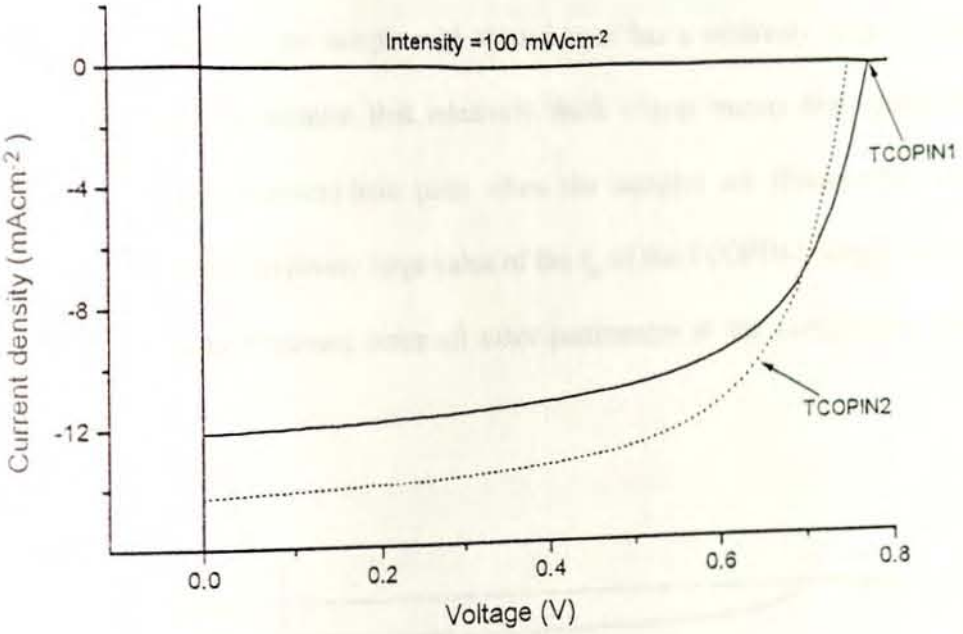

Figure 5. 2 The J-V characteristics of the TCOPIN1 and the TCOPIN2 solar cell samples.

Figure 5.2 shows the J-V characteristics of the TCOPIN1 and the TCOPIN2 when the samples are illuminated with light having an intensity of 100 $mWcm^{-2}$. The values of the different electrical parameters for each samples are shown in Table 5.1.

Sample	Intensity ($mWcm^{-2}$)	J_{sc} ($mAcm^{-2}$)	V_{oc} (V)	η (%)	FF
TCOPIN1	100	12.11	0.78	5.95	0.65
TCOPIN2	100	14.35	0.76	6.91	0.64

Table 5. 1 The J_{sc} , V_{oc} , η and FF of the samples.

It is observed that the values of the V_{oc} for the a-Si:H samples are close to each other. The V_{oc} is a function of the energy band gap of the material under consideration as it is expressed by Eqn. (2.25). Thus what is observed in the experiment is in agreement with the fact expressed by Eqn. (2.25). The slight difference in the V_{oc} between the samples is due to the difference in their i-layer thickness (i.e., recombination of carriers is more pronounced in the thicker sample than in the thinner one).

For the same intensity the sample with thick i-layer has a relatively large J_{sc} than that with thin i-layer. This is because that relatively thick i-layer means high probability for the formation of more electron-hole pairs when the samples are illuminated with the same intensity. Hence, the relatively large value of the J_{sc} of the TCOPIN2 sample can be attributed to the thick i-layer thickness since all other parameters of the samples are practically the same.

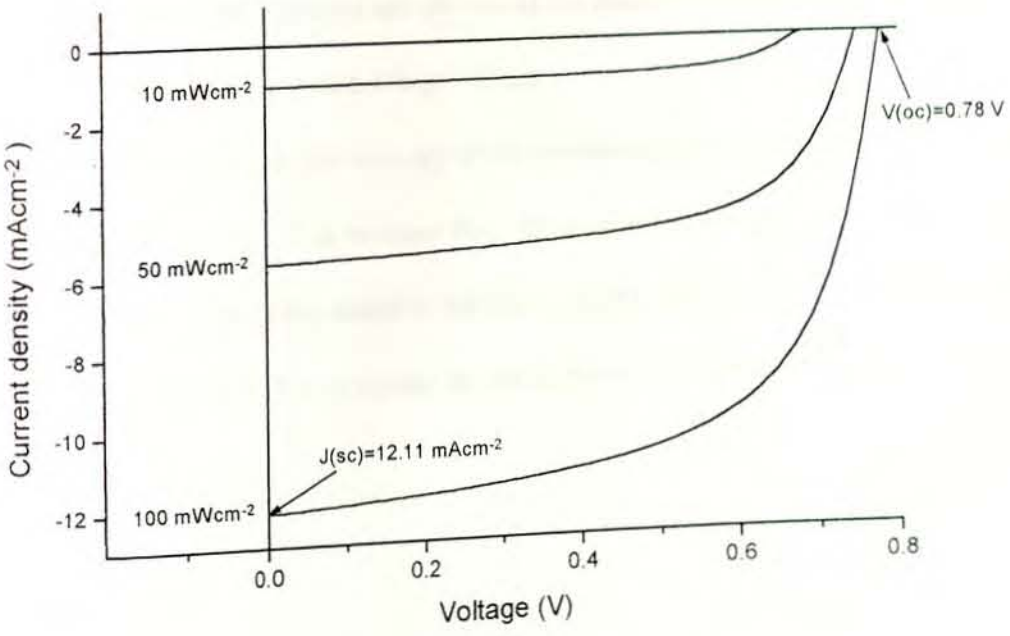

Figure 5. 3 The J-V characteristics of the TCOPIN1 sample.

The J-V characteristics of the TCOPIN1 sample, when it is illuminated with light having different intensities is shown in Fig. 5.3. The values of the different electrical parameters are tabulated in Table 5.2.

Sample	Intensity ($mWcm^{-2}$)	J_{sc} ($mAcm^{-2}$)	V_{oc} (V)	η(%)	FF
TCOPIN1	100	12.11	0.78	5.95	0.65
	50	5.67	0.75	5.42	0.64
	10	1.06	0.68	4.82	0.67

Table 5. 2 The values of the J_{sc}, V_{oc}, η and FF of the TCOPIN1 sample.

It is found that the J_{sc} is strongly dependent on the intensity of the incident light. When the intensity of the incident light is increased, the light generated current increases too. It is because that increasing the intensity of the incident light means increasing the photon flux which are capable of producing large number of electron-hole pairs (Section 2.8). In turn, the generated carriers (the electrons and the holes) are pushed by the built-in electrostatic field to the contacts where they produce a large current.

The decrease in the V_{oc} as the intensity of the incident light is decreased is small compared to the decrease in the J_{sc}. It is because that, for a given solar cell sample, the V_{oc} is mainly dependent on the type of the absorber material (a-Si:H) rather than on the intensity of the light incident on the sample. The variations in the fill factor with increasing intensity are negligibly small.

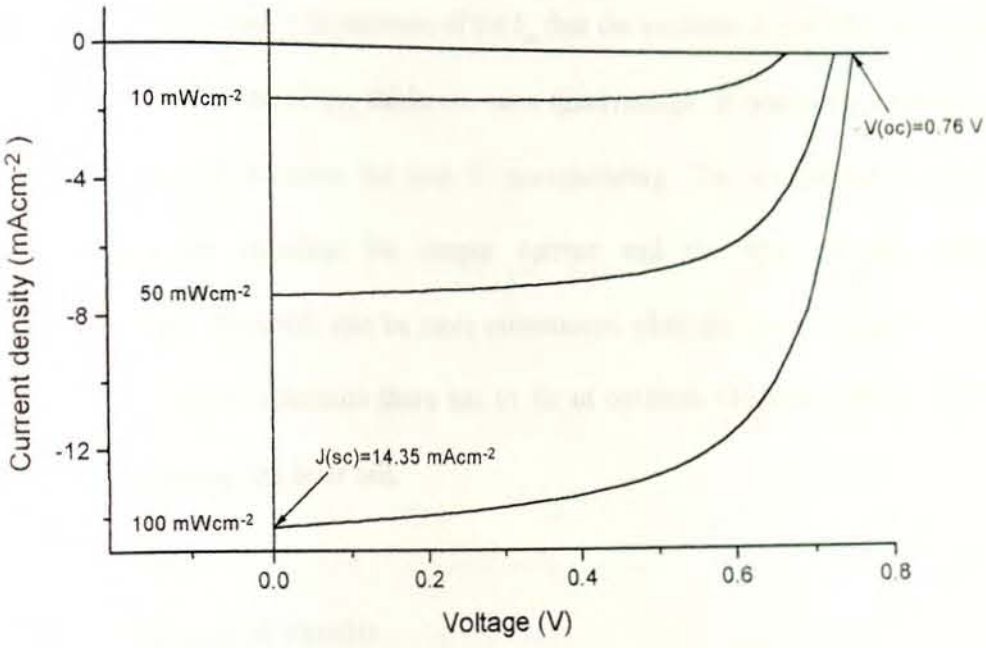

Figure 5. 4 The J-V characteristics of the TCOPIN2 sample.

Figure 5.4 depicts the J-V characteristics of the TCOPIN2 sample when it is illuminated with light of different intensities. The values of the J_{sc} , V_{oc} , η and FF are displayed in Table 5.3.

Sample	Intensity ($mWcm^{-2}$)	J_{sc} ($mAcm^{-2}$)	V_{oc} (V)	η(%)	FF
TCOPIN2	100	14.35	0.76	6.91	0.64
	50	7.4	0.73	6.88	0.64
	10	1.6	0.67	6.79	0.63

Table 5. 3 The values of the electrical parameters of the TCOPIN2 sample.

Similar to the TCOPIN1 sample, the J_{sc} strongly depends on the intensity while the dependence of the V_{oc} on the intensity is small compared to that of the J_{sc} . The variations in the values of the fill factors are found to be negligibly small.

The efficiency of the TCOPIN2 sample is found to be greater than that of the TCOPIN1. The cause for difference in efficiency is attributed to the difference in the i-layer thickness of the this suggest that as the i-layer thickness increases, the probability for the

generation of electron-hole pairs increases which results in an increase in the light generated current. It is mainly due to an increase of the J_{sc} that the variation in the efficiency is observed. However, increasing the i-layer thickness has a disadvantage. It needs more material to have thicker layer, which increases the cost of manufacturing. The recombination rate will also increase there by reducing the output current and the open circuit voltage. The Staebler-Wronski effect will also be more pronounced when the i-layer thickness is increased. Hence, under a given condition there has to be an optimum thickness of the different layer systems that make up the solar cell.

5. 3 Comparison of results

The efficiencies and the fill factors obtained by analysing the experimental data that are collected to determine the J-V characteristics curves of the solar cell samples, are presented and compared with reference values. The values tabulated below are for an intensity of 100 $mWcm^{-2}$ illumination of the samples.

Samples	Calculated efficiency (%)	Calculated fill factor
TCOPIN1	5.95	0.65
TCOPIN2	6.91	0.64

Table 5. 4 The calculated efficiencies and fill factors of the TCOPIN1 and the TCOPIN2 samples.

The efficiencies of the TCOPIN1 and the TCOPIN2 samples are small compared with the published value of 12.7 % [22], for a single cell structure . This low efficiency values are obtained because that the samples are prepared to investigate some of the optical and electrical properties of solar cells. Hence, not all the factors that are used to improve the efficiency of

solar cells are utilised in order to make optical investigation simple. To mention some of the properties of the samples: (i) the TCO deposited on the substrate is flat instead of rough. If the samples were assembled from rough TCO, the efficiencies would have been increased significantly, (ii) the surfaces of the samples are not textured. Surface texturing may have increased the efficiencies up to 2 % and (iii) antireflection coating is not present on the samples. If it were coated, the efficiencies would have been increased by up to 3 %. These and other factors may have resulted in the small value of the efficiencies of the samples compared with the reference value.

The deviation in the fill factor compared with the reference value of 0.74 [22] may have resulted because of the difference in the series and shunt resistances associated with the samples. Generally, the fill factors of the TCOPIN1 for different intensity of light illumination are slightly larger than that of the TCOPIN2. This may be due to the difference in the i-layer thickness. As the layer thickness increases the fill factor decreases due to the decrease in the electric field in the depletion region [15].

6. Conclusion

From the simulation of the transmittance spectra of the a-Si:H pin solar cells, the energy gaps, the refractive indices and the layer thickness of the different layers of the a-Si:H solar cells are determined. The fitted curves and the comparison of the fitted values with published results shows clearly that the Forouhi and Bloomer dielectric function model is effective in determining the above mentioned optical parameters. One of the advantages of using the Forouhi and Bloomer model is that it is possible to determine the energy gap and the refractive index of solar cell samples using only five fitting parameters for each layers. Besides, the Forouhi and Bloomer dielectric function is found to be more effective for the sample with thin i-layer than for that with thick i-layer. Hence, it is recommended to use this model to the investigation of the optical properties of individual layers of solar cells rather than a stack of layers.

From the J-V characteristics curves of the a-Si:H pin solar cell samples, it is found out that by increasing the i-layer thickness it is possible to increase the number of photogenerated electron hole pairs which in turn results to an increase in the J_{sc}. In fact, there has to be an optimum thickness as it is not possible to increase the thickness indefinitely to generate more current. Illuminating the samples with light of different intensities also resulted to an increase in the photogenerated current with an increase of the intensity of light. But, the increase in the V_{oc} with intensity is found to be insignificant compared to that of the J_{sc}.

References

[1] S. J. Fonash, Solar Cell Device Physics, Academic Press, New York (1981).

[2] M. A. Green, Solar Cells, Prentice-Hall, Inc., Englewood Cliffs, N. J., (1982).

[3] A. Madan, Physics and Applications of Amorphous Semiconductors; Utilisation of Amorphous Silicon in Solar Cell Applications, World Scientific Publishing Co Pte Ltd., (1988) pp. 65-103.

[4] H. Fritzsche, Physics and Applications of Amorphous Semiconductors; Thermal Equilibration and Heterogeneous Structure of Hydrogenated Amorphous Silicon, World Scientific Publishing Co Pte Ltd., (1988) pp. 65-103.

[5] N. Maley, Interference-Free Determination of the Absorption Coefficient of Amorphous Silicon Thin Films, Jpn. J. Appl. Phys. Vol. 31 (1992) pp. 768-769.

[6] W. Fuhs, Electronic Properties of Plasma-Deposited Amorphous Semiconductor Films, Chapter 3, pp. 55-56.

[7] E. Hecht, A. Zajac, Optics, Addison-Wesley Publishing Comp., Inc., (1974) pp. 71-80.

[8] T. Markvart, Solar Electricity, University of Southampton, (1994).

[9] A. R. Forouhi, I. Bloomer, Optical Dispersion Relations for Amorphous Semiconductors and Amorphous Dielectrics, Phys. Rev. B, Vol. 34, No. 10, (1986) pp. 7018-7026.

[10] A. R. Forouhi, I. Bloomer, Handbook of Optical Constants of Solids II, Academic Press (1991) pp. 151-175.

[11] W. Theis, The SCOUT through CAOS-a system for doing optics by computer, Aachen, (1994) pp. 1-70.

[12] Amensisa Abdi, M. Sc. Thesis (AAU), Optical Characterisation of Thin Films for Solar Cell Application (1995).

[13] J. R. Taylor, An Introduction to Error Analysis, Oxford University Press, (1982) pp. 218-237

[14] Perkin Elmer, Lambda 19 Spectrometer manual, user documentation, volume 1 of 3.

[15] F. B. Ellis Jr., A. E. Delahoy, Optical Properties of Hydrogenated Amorphous Silicon Based Solar Cells, Solar Energy Materials 13 , North-Holland, Amsterdam, (1986) pp. 109-132.

[16] R. R. Arya, Physics and Applications of Amorphous Semiconductors, High Efficiency Amorphous Silicon Based Solar Cells, World Scientific Publishing Co Pte Ltd., (1988) pp. 263-277.

[17] S. C. Jain and S. Radhakrishana, Physics of Semiconductor Devices, Proceedings of the Fourth International Workshop, Madras (India), 1987.

[18] R. J. Schwartz, G. B. Turner, J. W. Park, J. L. Gray, "Physics of Amorphous Semiconductor Devices", vol. 763 (1987) pp. 126.

[19] T. Eickhoff, H. Stiebig, "Modellierung der Spektralen Empfindlichkeit von α-Si:H Solarzellen", Photovoltaik 3, Forschungsverbund Sonnenenergie, Themen 95/96, Koeln (1996)

[20] R. Plaettner, W. Stetter, P. Kochler, "Transparent Conductive Tin-Oxide Layers for Thin Film Solar Cells", Siemens Forsch.-u. Entwickl. Ber., Bd. 17 (1988)

[21] F. Leblanc, J. Perria, E. Cornil, J. Schmitt, "Experimental Characterisation and Optical Modelling of absorption and light trapping in α-Si:H Solar Cells on Textured TCO", Material Research Society Proc. Vol. 258 (1992)

[22] Martin A. Green, Keith Emery, Klaus Bucher and David L. King, "Solar Cell Efficiency Tables", in "Progress in Photovoltaics Research and Applications", Vol. 3, No. 1, (1995) pp. 51-54.

Declaration

I, the undersigned, declare that the thesis is my original work, has not been presented for a degree in any other university and that all sources of material used for the thesis have been duly acknowledged.

Name: Belayneh Mesfin

Signature: _____

Place and date of submission: Addis Ababa University, Department of Physics, June 1998.

This thesis has been submitted for examination with my approval as university advisor.

Name: Ulrich Stutenbaeumer (Ph.D.)

Signature: _____

Date: 19.06.98